

Two-parameter estimation with three-mode NOON state in a symmetric three-well

Fei Yao,¹ Yi-Mu Du,¹ Haijun Xing,^{1,*} and Libin Fu^{1,†}

¹*Graduate School of China Academy of Engineering Physics, Beijing 100193, China*

We propose a theoretical scheme to realize two-parameter estimation via a Bose-Einstein condensates confined in a symmetric triple-well. The three-mode NOON state is prepared adiabatically as the initial state. Two phase differences between the wells are two parameters to be estimated. With the help of classical and quantum Fisher information, we study the sensitivity of the triple-well on estimating two phase parameters simultaneously. The result shows that the precision of simultaneous estimation of two parameters in a triple-well system can reach the Heisenberg scaling.

I. INTRODUCTION

Quantum metrology has attracted considerable interest in recent years, due to its wide application in basic science as well as applied technology. The quantum parameter estimation theory [1, 2] and Fisher information, as crucial tools in quantum metrology, provide theoretical bases for us to study enhancing the accuracy of parameter estimation with quantum resources. In the previous researches on the parameter estimation, the single-parameter estimation has been well studied and a series of achievements have been made [3–5], such as gravitational wave detection [6], magnetometry [7–9], atomic clocks [10–14].

Although the single parameter estimation plays an important role in many applications, it is often necessary to estimate multiple parameters simultaneously in practical problems. It can be seen that studying the multiparameter estimation is an urgent need for effectively solving the actual parameter estimation problems. Recently, the studies on the multi-parameter estimation have attracted more attentions [15–27]. Most of these works aim to quantifying and enhancing the precision of multi-parameter estimation in a general framework. There are a few studies on specific schemes for realizing the multi-parameter estimation. Therefore, we consider proposing a theoretical scheme to achieve simultaneous estimation of multiple parameter.

The double-well potential, as a classical model, has been widely used in Bosonic Josephson junction [28, 29], matter-wave interferometry [30–44] and so on. With the development of the techniques for manipulating ultracold atoms, a variety of double-well atom interferometers [30, 35] have been introduced to estimate single parameter. As an extension of the single parameter estimation with the double-well, we come up with using a symmetrical triple-well [45–49] that confined bosonic atoms to study the two-parameter estimation.

Our measurement scheme consists of four stages: initialization, parameterization, rotation and measurement. Since the use of quantum entanglement resources [50–

52] can enhance the precision of parameter estimation, we prepare the condensates into the three-mode NOON state adiabatically, which is the initial state. The parameters to be estimated are two phase differences between the wells caused by the external field. Regarding the measurement method, the particle number projection measurement is chosen. In order to study the accuracy of the measurement scheme with triple-well system, we calculate the quantum Fisher information matrix (QFIM) and classical Fisher information matrix (CFIM) on two parameters. By comparing the CFIM and QFIM, we find that the measurement rotation time has a great effect on the measurement precision, and the optimal rotation time is given. In addition, the result shows that, the optimal measurement precision of our scheme can approach the Heisenberg scaling.

The paper is organized as follows. In Sec. II, the model and basic measurement theory are introduced. In Sec. III, measurement scheme of estimating two parameters with the triple-well system is given, including initial state preparation, parameterization and projection measurement. By analyzing the CFIM and QFIM on two estimated parameters, the optimal measurement conditions are given and the optimal measurement precision is obtained. In Sec. III, we give a summary.

II. MODEL AND BASIC THEORY

In this section, we sketch our scheme. We confine N Bose-Einstein condensed atoms in a symmetric triple-well system(STWS) [45–49], as seen in Fig. 1-(a). The Hamiltonian is

$$\hat{H} = -J \sum_{i=1}^3 (\hat{a}_i^\dagger \hat{a}_j + h.c.) + U \sum_{i=1}^3 \hat{n}_i (\hat{n}_i - 1), \quad (1)$$

with $j = (i+1)\bmod 3 + 1$. The operators $\hat{a}_i^\dagger (\hat{a}_i)$ and $\hat{n}_i = \hat{a}_i^\dagger \hat{a}_i$ are the creation(annihilation) operator and the particle-number operator for bosonic atoms in the i -th well, respectively. J is the tunnelling strength between the wells. U is the atomic on-site interaction, and $U > 0$ ($U < 0$) imply a repulsive (attractive) interaction. Here, we consider attractive interaction. In this model, the total atom number $N = \sum_{i=1}^3 n_i$ is conserved.

*Electronic address: hjxing@gscap.ac.cn

†Electronic address: libfu@gscap.ac.cn

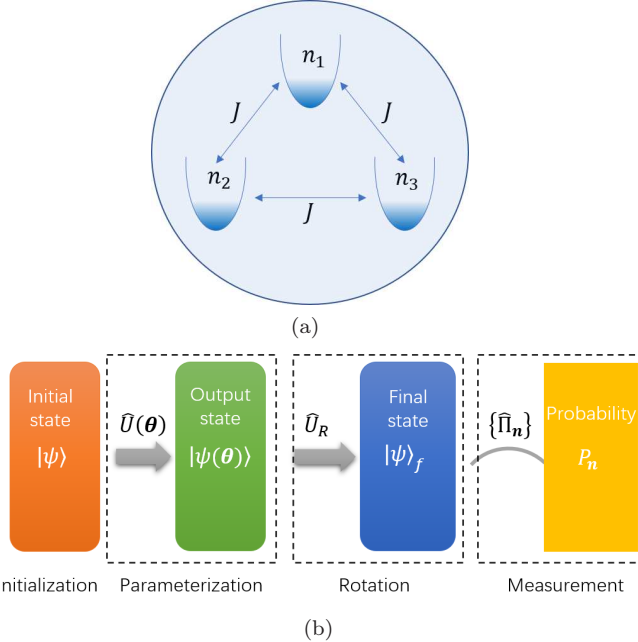


FIG. 1: (Color online) (a) The Schematic diagram of a symmetric triple-well trapped Bose atoms. (b) General framework of multiparameter estimation.

The system state can be expanded in basis of Fock state $\{|n_1, n_2, n_3\rangle\}$, with n_i particle in the i -th well, $i = 1, 2, 3$.

Assuming that the STWS is in an initial state $|\psi\rangle$, place it in a uniform external field, and the three potential wells obtain phases ϕ_1 , ϕ_2 and ϕ_3 , respectively. We consider the simultaneous estimation of two phase differences $\theta_1 = \phi_1 - \phi_3$ and $\theta_2 = \phi_2 - \phi_3$. The procedures of our scheme are shown as follows(see Fig. 1-(b)).

- Initialization: Prepare the initial state $|\psi\rangle$.
- Parameterization: The initial state $|\psi\rangle$ is parameterized and the output state $|\psi(\boldsymbol{\theta})\rangle = \hat{U}(\boldsymbol{\theta})|\psi\rangle$ is obtained. Here, $\hat{U}(\boldsymbol{\theta})$ is a unitary transformation and $\boldsymbol{\theta} = (\theta_1, \theta_2)$ is a vector parameter.
- Rotation: Rotate the output state $|\psi(\boldsymbol{\theta})\rangle$ and obtain the measurable final state

$$|\psi_f\rangle = \hat{U}_R|\psi(\boldsymbol{\theta})\rangle. \quad (2)$$

- Measurement: Given a set of projective measurements $\{\hat{\Pi}_n\}$ (n representing the possible result), the probability of observing the sequence n , which conditioned to the vector parameter $\boldsymbol{\theta}$ is

$$P_n = {}_f\langle\psi|\hat{\Pi}_n|\psi\rangle_f. \quad (3)$$

Vector $\boldsymbol{\theta}$ is estimated based on the measurement results. The accuracy of estimation will be discussed with the help of Fisher information. For the measurement probability shown in Eq. (3), the matrix elements of CFIM \mathbf{F}^c is

$$\mathbf{F}_{\mu,\nu}^c = \sum_n \frac{(\partial_\mu P_n)(\partial_\nu P_n)}{P_n}, \quad (4)$$

with $\partial_\mu = \partial/\partial\theta_\mu$ and $\mu, \nu = 1, 2$. Obviously, the CFI depends on the measurement scheme, and it gives the best accuracy that can be achieved by the corresponding measurement scheme. According to the multiparameter quantum estimation theory [1, 2, 22, 25], the precision of vector parameter $\boldsymbol{\theta}$ is determined by the covariance matrix $\boldsymbol{\Sigma}$ ($\boldsymbol{\Sigma}_{\mu,\nu} = \text{Cov}(\theta_\mu, \theta_\nu)$). It is bounded by the QFIM \mathbf{F}^q via the quantum Cramér-Rao inequality (QCRI)

$$\boldsymbol{\Sigma} \geq (\mathbf{F}^c)^{-1} \geq (\mathbf{F}^q)^{-1}, \quad (5)$$

where the matrix elements of \mathbf{F}^q is defined as

$$\mathbf{F}_{\mu,\nu}^q = 4\text{Re}[\langle\partial_\mu\psi(\boldsymbol{\theta})|\partial_\nu\psi(\boldsymbol{\theta})\rangle - \langle\partial_\mu\psi(\boldsymbol{\theta})|\psi(\boldsymbol{\theta})\rangle\langle\psi(\boldsymbol{\theta})|\partial_\nu\psi(\boldsymbol{\theta})\rangle]. \quad (6)$$

QFIM depended on the initial state and parameterization process. Here, \mathbf{F}^c and \mathbf{F}^q are assumed invertible.

Following the standard methods, we measure the (inverse of the) estimation's precision with $\text{tr}\boldsymbol{\Sigma} = \sum_\mu \delta^2 \theta_\mu$. According to the QCRI, we have

$$\text{tr}\boldsymbol{\Sigma} \geq \text{tr}[(\mathbf{F}^c)^{-1}] \geq \text{tr}[(\mathbf{F}^q)^{-1}], \quad (7)$$

where attainability of the second equality relies on the estimation (measurements). In this article, we assume the first equality can always be attained, e.g., via the maximally likelihood estimation [1, 53, 54]. And the (inverse of the) estimation's *precision* is thus measured by $\text{tr}[(\mathbf{F}^c)^{-1}]$. Eq. (7) shows that the QFI matrix determines a lower bound on this precision. Therefore, we further measure the quality of the measurement scheme with the gap

$$\Delta = \text{tr}[(\mathbf{F}^c)^{-1}] - \text{tr}[(\mathbf{F}^q)^{-1}]. \quad (8)$$

The Eq. (8) shows that the smaller Δ is, the better the measurement scheme is, and the more accurate the parameter estimation is.

III. TWO PARAMETER ESTIMATION WITH THE STWS

A. The initial state preparation

In quantum metrology, the quantum entanglement resources are often used to improve measurement accuracy. The studies in Ref. [35, 56–58] shows that, the quantum entanglement of a GHZ or NOON state lead to the Heisenberg limit. In our triple-well system, one can prepare the *three-mode NOON state*

$$|\psi\rangle = \frac{1}{\sqrt{3}} (|N, 0, 0\rangle + |0, N, 0\rangle + |0, 0, N\rangle) \quad (9)$$

as the initial state of the system. In this section, we will discuss the preparation of the initial state in the Eq. (9).

Before introduce the preparation, we briefly recall the eigenspectrum of the Hamiltonian (1). As shown in

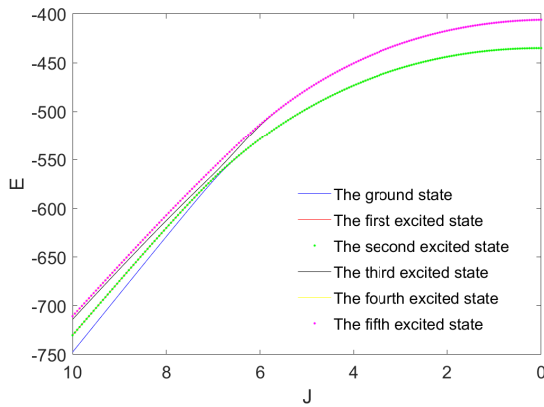


FIG. 2: (Color online) Energy spectrum for different J . Here we set $U = -0.5$ and $N = 30$. Because of the large number of energy levels, only the lowest six energy levels are given.

Fig. 2, in the case of $J = 0$ and $U < 0$, the ground state is threefold degenerate ($|e_1\rangle = |N, 0, 0\rangle$, $|e_2\rangle = |0, N, 0\rangle$ and $|e_3\rangle = |0, 0, N\rangle$), because of attractive interaction. In the strong coupling limit ($J/|U| \gg 1$), we focus on the lowest three energy levels. The Fig. 2 shows that, the first excited state and the second excited state of the system are degenerate due to the symmetry of the STWS itself. At the same time, since the coupling strength in the Hamiltonian (1), the ground state and the first excited state are non-degenerate. Furthermore, from the Fig. 2, as J decreases slowly to zero, the energy gap between the ground state and the first excited state decreases gradually.

Next, we demonstrate the preparation of the initial state by Fig. 3. The target state in Eq. (9) can be obtained by preparing the ground state in the strong coupling limit ($J/|U| \gg 1$), and then slowly decreasing the coupling strength J to zero, as indicated in Fig. 3-(a). The Fig. 3-(a) shows the fidelity $|\langle\psi(t)|\psi\rangle|^2$ of the evolving state $|\psi(t)\rangle$ from $J = 10$ to 0. This is an adiabatic evolution process, and the change rate of parameter J can be adjusted according to the requirements of adiabatic fidelity [55]. In order to show the initial state more clearly, the particle distribution of the ground state at $J = 10$ and $J = 0$ are plotted in Fig. 3-(b) and Fig. 3-(c), respectively. In Fig. 3-(b), the particle distribution is approximately a Gaussian distribution. In Fig. 3-(c), the particles have an equal probability distribution in states $|N, 0, 0\rangle$, $|0, N, 0\rangle$ and $|0, 0, N\rangle$. And the vanishing of the relative phases between the three states is verified numerically. It shows the ground state Fig. 3-(c) is the target initial state to be prepared.

B. Parameterization and the QFI

In the last section, the three-mode NOON state is prepared as the initial state of STWS via adiabatic evolution. Setting the STWS with the prepared initial state

into an external field, the state $|\psi\rangle$ is parameterized and evolved into the output state as

$$|\psi(\boldsymbol{\theta})\rangle = \frac{1}{\sqrt{3}}(\mathbf{e}^{-iN\theta_1}|N, 0, 0\rangle + \mathbf{e}^{-iN\theta_2}|0, N, 0\rangle + |0, 0, N\rangle). \quad (10)$$

where $\boldsymbol{\theta} = (\theta_1, \theta_2)$ is the vector parameter to be estimated.

Substituting the Eq. (10) into the Eq. (6), we have the QFIM

$$\mathbf{F}^q = \frac{4N^2}{9} \begin{pmatrix} 2 & -1 \\ -1 & 2 \end{pmatrix}. \quad (11)$$

It is observed from above equation that the QFIM only depends on the total particle number N , independent of $\boldsymbol{\theta}$. Furthermore, based on the QCRI in Eq. (7), we have

$$\langle\Delta\boldsymbol{\theta}\rangle^2 \geq \text{tr}[(\mathbf{F}^q)^{-1}] \sim O(\frac{1}{N^2}), \quad (12)$$

where $\langle\Delta\boldsymbol{\theta}\rangle^2 \equiv \langle\Delta\theta_1\rangle^2 + \langle\Delta\theta_2\rangle^2$ is total variance of θ_1 and θ_2 . The Eq. (12) indicates the upper bound of precision of estimating $\boldsymbol{\theta}$ can approach the Heisenberg scaling.

C. Projective measurement and the CFIM

We have discussed the theoretical limit of the sensitivity via the QFIM. However, the accessible sensitivity highly depends on the measurement scheme. In this section, we focus on the measurement precision which is characterized by the CFIM.

We measure the particle number in each of wells on the final state. It is depicted by the projection operator

$$\{\hat{\Pi}_{\mathbf{n}}\} = \{|n_1, n_2, n_3\rangle\langle n_1, n_2, n_3|\}, \quad (13)$$

with $\mathbf{n} = (n_1, n_2, n_3)$. However, performing this measurement on the parameterized state in Eq. (10) directly will eliminate the phases. One thus incapable of inferring the parameter $\boldsymbol{\theta}$. Hence, we rotate the output state before the measurement with

$$\hat{U}_R = \exp[-i\hat{H}_R t], \quad (14)$$

where t is rotation time and

$$\hat{H}_R = -J \sum_{i=1}^3 (\hat{a}_i^\dagger \hat{a}_j + h.c.), \quad (15)$$

with $j = (i+1)\bmod 3 + 1$. The value of J is fixed throughout the rotation operation. This Hamiltonian can be realized approximately by tuning the hoping to $J \gg UN$. Based on the Eqs. (2), (10), and (14), we have the rotated final state as (see Appendix A)

$$|\psi\rangle_f = \sum_{n_1, n_2, n_3} \sum_{i=1}^3 C e^{-iN\theta_i} [\xi(\tau)]^{n_i} [\eta(\tau)]^{N-n_i} |n_1, n_2, n_3\rangle \quad (16)$$

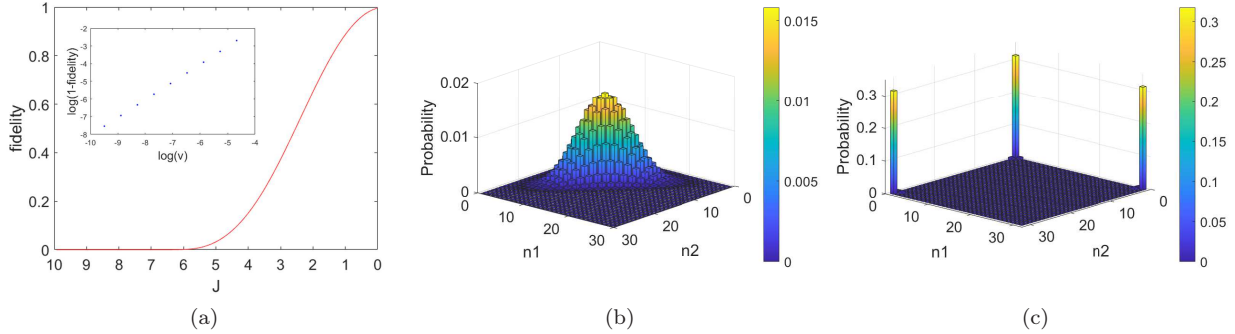


FIG. 3: (Color online) (a) The fidelity $|\langle \psi(t) | \psi \rangle|^2$ varies with J , where $J = J_0 - vt$ with $J_0 = 10$, $v = 0.0039$. $|\psi\rangle$ is the target three-mode NOON state and $|\psi(t)\rangle$ is the evolving state from the system ground state. The inset shows the performance of the state preparation versus the quantity $v = J$ which is proportional to the adiabatic parameter. (b-c) The particle distribution of the ground state in basis $|n_1, n_2, n_3\rangle$. (b) The ground state at $J = 10$. (c) The ground state at $J = 0$ is an entangled state $\frac{1}{\sqrt{3}}(|N, 0, 0\rangle + |0, N, 0\rangle + |0, 0, N\rangle)$ approximately. The phase values of states $|N, 0, 0\rangle$, $|0, N, 0\rangle$ and $|0, 0, N\rangle$ are all 0.6127. Here, $U = -0.5$ and $N = 30$.

with $\theta_3 = 0$, $C = (\frac{N!}{3^{2N+1}n_1!n_2!n_3!})^{1/2}$, $\xi(\tau) = e^{2i\tau} + 2e^{-i\tau}$, $\eta(\tau) = e^{2i\tau} - e^{-i\tau}$ and the generalized rotation time $\tau = Jt$ (its unit is $1/J$).

Applying the projector in Eq. (13) to the final state in Eq. (16), we have the probability distribution

$$\begin{aligned}
 P_n &= {}_f \langle \psi | n_1, n_2, n_3 \rangle \langle n_1, n_2, n_3 | \psi \rangle_f \\
 &= C \left\{ \sum_{i=1}^3 [z(\tau)]^{n_i} [s(\tau)]^{N-n_i} + \sum_{i \neq j \neq k} 2(-1)^{N-n_i} [s(\tau)]^{n_i} \operatorname{Re} [\gamma_\theta [x(\tau)]^{n_j} [x^*(\tau)]^{n_k}] \right\}
 \end{aligned} \tag{17}$$

with $i, j, k \in \{1, 2, 3\}$, $z(\tau) = 1 + 8\cos^2(3\tau/2)$, $s(\tau) = 4\sin^2(3\tau/2)$, $x(\tau) = 1 - 2e^{-3i\tau} + e^{3i\tau}$, $\gamma_\theta = \exp[-iN(\theta_j - \theta_k)]$, and $\theta_3 = 0$.

Inserting Eq. (17) into Eq. (4), one can acquire the CFIM which depends on the estimated vector θ and τ . We thus denote it as $\mathbf{F}^c(\theta, \tau)$ for accuracy. It indicates, to optimize the precision of the estimation, we should select the appropriate θ_1 , θ_2 and τ . As follows, we utilize the gap Δ in Eq. (8) to analyze the effects of θ_1 , θ_2 and τ on the measurement precision.

Firstly, we discuss the relations of Δ on θ_1 and θ_2 with a given rotation time τ . The numerical results are shown as Fig. 4, here only one period is shown. We observe that $\ln(\Delta)$ highly depends on θ_1 and θ_2 . For a given τ , the maximal precision can only be achieved in several points "●". Luckily, with enough prior information, we can shift the estimand to the vicinity of these points to approach the maximal precision.

Secondly, by comparing Fig. 4-(a) and Fig. 4-(b), we find that, not only the maximal precision, but also the parameter θ taking the maximal precision are highly dependent on the rotation time τ .

For rotation time is also controllable, we can optimize the precision over τ . For convenience, we define

$$\delta(\tau) = \min_{\{\theta_1, \theta_2\}} [\ln(\Delta)], \tag{18}$$

to study the effect of τ on the minimum value of $\ln \Delta$. We plot $\delta(\tau)$ numerically in Fig. 5-(a). It shows that $\delta(\tau)$ varies periodically with τ . There is a large period duration 2π containing a small period duration $2\pi/3$. More importantly, the $\delta(\tau)$ takes the minimum value at points

$$\tau \approx \frac{(2k+1)\pi}{3} \pm \frac{\pi}{9}, \tag{19}$$

where k is a natural number. We further show its validity numerically in Fig. 5-(b), that indicates the optimal measurement precision is obtained, when τ is set as in Eq. (19).

To evaluate the quality of the optimal precision, we study the CFIM at $\tau = 2\pi/9$ both numerically and analytically. Firstly, we search the minimum of $\operatorname{tr}[(\mathbf{F}^c)^{-1}]$ via numerical optimization over the phase parameter θ .

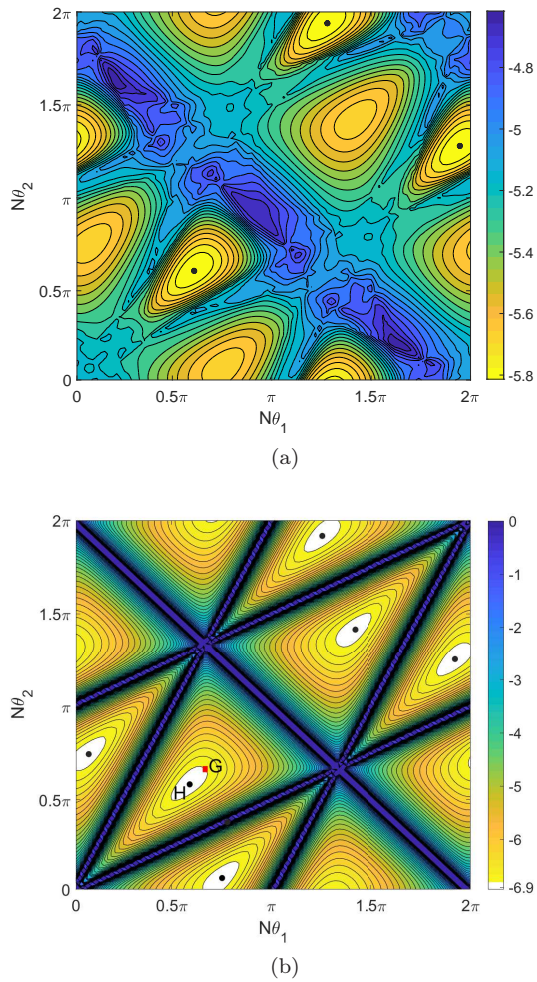


FIG. 4: (Color online) $\ln(\Delta)$ varies with θ_1, θ_2 at fixed τ . Here we set $N = 30$. (a) $\tau = 0.2\pi$. (b) $\tau = 2\pi/9$. The optimal precision is obtained in the vicinity of point H (white area), and the precision at point $G = (2\pi/3, 2\pi/3)$ is approximately equal to that at the point H . The blue areas in Fig. 4-(b) represent areas with $\ln(\Delta) \geq 0$.

The result is illustrated as function of N^2 in Fig. 6, which shows a linear relationship

$$\min_{\{\theta_1, \theta_2\}, \tau} \text{tr}[(\mathbf{F}^c)^{-1}] \propto \frac{1}{N^2} \quad (20)$$

approximately. It indicates the Heisenberg scaling precision. To show it more concretely, we further analytically calculate the precision of a set of exemplified states, whose parameters are $\boldsymbol{\theta}_{G_N}$ with $N\theta_1 = N\theta_2 = 2(N+1)\pi/3$. As exemplified by point G in Fig. 4, these states locate in the vicinity of the optimal states (H). The analytical results in Appendix B shows that the CFIM of these exemplified states are

$$\mathbf{F}^c(\boldsymbol{\theta}_{G_N}, \frac{2\pi}{9}) = \frac{N^2}{3} \begin{pmatrix} 2 & -1 \\ -1 & 2 \end{pmatrix}, \quad (21)$$

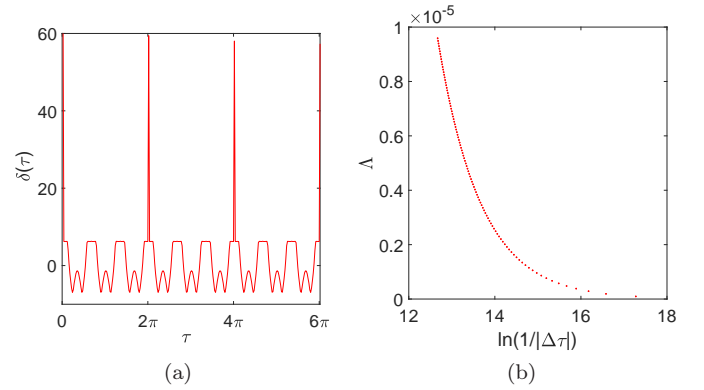


FIG. 5: (Color online) (a) $\delta(\tau)$ varies with rotation evolution time τ . (b) Δ varies with $1/|\Delta\tau|$. Here $\Delta = \delta(\tau) - \delta(\tau = 2\pi/9J)$, $|\Delta\tau| = |\tau - 2\pi/9|$. Δ decreases to zero with $1/|\Delta\tau|$ increases to infinity ($\Delta\tau \rightarrow 0$). Here we set $N = 30$.

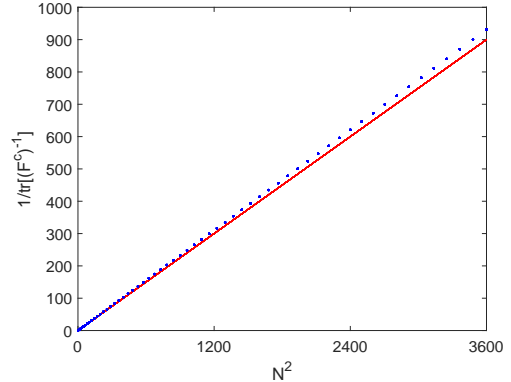


FIG. 6: (Color online) Precision $(1/\text{tr}[(\mathbf{F}^c)^{-1}])$ as a function of particle number N^2 . Here, we set $\tau = 2\pi/9$. The blue dotted line denotes the optimal precision acquired via numerical optimization. The red solid line is analytical result at $\boldsymbol{\theta}_{G_N}$, which reads $\text{tr}[(\mathbf{F}^c)^{-1}] = 4/N^2$.

which present us the precision $\text{tr}[(\mathbf{F}^c)^{-1}] = 4/N^2$. And as shown by Fig. 6, the optimal states behaves a better scaling.

The Eqs. (20) and (21) show that, with the proposed measurement scheme, the optimal measurement precision of two parameters θ_1 and θ_2 shows the Heisenberg scaling. This indicates that our proposed theoretical scheme of using the triple-well system to estimate two parameters simultaneously is feasible. Furthermore, as indicated by Fig. 4-(b) and Fig. 6, the precision is robust around the optimal states, e.g., the state G still have a relative high precision with a Heisenberg scaling. It tremendous lower the demands for practical studies, which relieve the constrain of working point from "H" to, e.g., the white zoom in Fig. 4-(b). With a relative bigger acceptance zoom of the parameter shifts, the demands for the prior information about $\boldsymbol{\theta}$ is also highly reduced.

IV. CONCLUSION AND DISCUSSION

In this work, we have proposed a theoretical scheme for estimating two-parameter via a Bose-Einstein condensate confined in a symmetric triple-well. The three-mode NOON state is prepared adiabatically as the initial state. Two phase differences between the wells are parameters to be estimated, which are encoded into the initial state via the external fields. For the specific measurement method, we take the particle number projection measurement in each of the wells. Moreover, a rotation operation is adopted on the output state before the measurement. To study the sensitivity of the estimation, we have calculated the QFIM and CFIM on the two phases. By optimizing the rotation time, we have found that the op-

timal precision approaches the Heisenberg scaling. Our scheme would be instrumental in providing theoretical guidance for experimental research, e.g., it has potential applications in measuring the external field with multiple components.

V. ACKNOWLEDGMENTS

Fei Yao thanks Peng Wang for the helpful discussion. This work was supported by the National Natural Science Foundation of China (NSFC) (No. 12088101, Grant No. 11725417, and Grant No. U1930403) and Science Challenge Project (Grant No. TZ2018005).

Appendix A: The derivation of the rotated final state

The parameterized output state is

$$|\psi(\theta)\rangle = \frac{1}{\sqrt{3}} (\exp[-iN\theta_1] |N, 0, 0\rangle + \exp[-iN\theta_2] |0, N, 0\rangle + |0, 0, N\rangle). \quad (\text{A1})$$

The output state will be rotated by the rotated operator $\hat{U}_R = \exp[-i\hat{H}_R t]$. Firstly, the Hamiltonian $\hat{H}_R = -\frac{1}{2}J \sum_{i,j=1, i \neq j}^3 (\hat{a}_i^\dagger \hat{a}_j + h.c.)$ can be diagonalized in the basis

$$\begin{pmatrix} \alpha_1 \\ \alpha_2 \\ \alpha_3 \end{pmatrix} = \frac{1}{\sqrt{3}} \begin{pmatrix} 1 & 1 & 1 \\ 1 & e^{i2\pi/3} & e^{-i2\pi/3} \\ 1 & e^{-i2\pi/3} & e^{i2\pi/3} \end{pmatrix} \begin{pmatrix} a_1 \\ a_2 \\ a_3 \end{pmatrix} \quad (\text{A2})$$

to give

$$\hat{H}_R = J \left(-2\alpha_1^\dagger \alpha_1 + \alpha_2^\dagger \alpha_2 + \alpha_3^\dagger \alpha_3 \right). \quad (\text{A3})$$

And then, the output state $|\psi(\boldsymbol{\theta})\rangle$ can be transformed into the eigenbasis vector of \hat{H}_R via the Eq. (A2). The transformation of $|\psi(\boldsymbol{\theta})\rangle$ is given as below,

$$\begin{aligned}
|\psi\rangle_f &= \hat{U}_R |\psi(\boldsymbol{\theta})\rangle' \\
&= \exp \left[-iJt \left(-2\alpha_1^\dagger \alpha_1 + \alpha_2^\dagger \alpha_2 + \alpha_3^\dagger \alpha_3 \right) \right] |\psi(\boldsymbol{\theta})\rangle \\
&= \exp [-iJt (-2\hat{n}_{\alpha 1} + \hat{n}_{\alpha 2} + \hat{n}_{\alpha 3})] \frac{1}{\sqrt{3^{N+1} N!}} \{ \exp [-iN\theta_1] (\alpha_1^\dagger + \alpha_2^\dagger + \alpha_3^\dagger)^N |0, 0, 0\rangle \\
&\quad + \exp [-iN\theta_2] (\alpha_1^\dagger + e^{i2\pi/3} \alpha_2^\dagger + e^{-i2\pi/3} \alpha_3^\dagger)^N |0, 0, 0\rangle + (\alpha_1^\dagger + e^{-i2\pi/3} \alpha_2^\dagger + e^{i2\pi/3} \alpha_3^\dagger)^N |0, 0, 0\rangle \} \\
&= \frac{1}{\sqrt{3^{N+1} N!}} \{ \exp [-iN\theta_1] (\alpha_1^\dagger + e^{2iJt} \alpha_1^\dagger + e^{-iJt} \alpha_2^\dagger + e^{-iJt} \alpha_3^\dagger)^N |0, 0, 0\rangle \\
&\quad + \exp [-iN\theta_2] (\alpha_1^\dagger + e^{2iJt} \alpha_1^\dagger + e^{i2\pi/3} e^{-iJt} \alpha_2^\dagger + e^{-i2\pi/3} e^{-iJt} \alpha_3^\dagger)^N |0, 0, 0\rangle \\
&\quad + (\alpha_1^\dagger + e^{2iJt} \alpha_1^\dagger + e^{-i2\pi/3} e^{-iJt} \alpha_2^\dagger + e^{i2\pi/3} e^{-iJt} \alpha_3^\dagger)^N |0, 0, 0\rangle \} \\
&= \frac{1}{\sqrt{3^{N+1} N!}} \{ \exp [-iN\theta_1] [(e^{2iJt} + 2e^{-iJt}) \alpha_1^\dagger + (e^{2iJt} - e^{-iJt}) (\alpha_2^\dagger + \alpha_3^\dagger)]^N |0, 0, 0\rangle \\
&\quad + \exp [-iN\theta_2] [(e^{2iJt} + 2e^{-iJt}) \alpha_2^\dagger + (e^{2iJt} - e^{-iJt}) (\alpha_1^\dagger + \alpha_3^\dagger)]^N |0, 0, 0\rangle \\
&\quad + [(e^{2iJt} + 2e^{-iJt}) \alpha_3^\dagger + (e^{2iJt} - e^{-iJt}) (\alpha_1^\dagger + \alpha_2^\dagger)]^N |0, 0, 0\rangle \} \\
&= \sum_{n_1, n_2, n_3} \sqrt{\frac{N!}{3^{2N+1} n_1! n_2! n_3!}} \{ \exp [-iN\theta_1] (e^{2iJt} + 2e^{-iJt})^{n_1} (e^{2iJt} - e^{-iJt})^{n_2+n_3} \\
&\quad + \exp [-iN\theta_2] (e^{2iJt} + 2e^{-iJt})^{n_2} (e^{2iJt} - e^{-iJt})^{n_1+n_3} \\
&\quad + (e^{2iJt} + 2e^{-iJt})^{n_3} (e^{2iJt} - e^{-iJt})^{n_1+n_2} \} |n_1, n_2, n_3\rangle \\
&= \sum_{n_1, n_2, n_3} \sum_{i=1}^3 \sqrt{\frac{N!}{3^{2N+1} n_1! n_2! n_3!}} \exp [-iN\theta_i] (e^{2iJt} + 2e^{-iJt})^{n_i} (e^{2iJt} - e^{-iJt})^{N-n_i} |n_1, n_2, n_3\rangle, \quad (A4)
\end{aligned}$$

where $\theta_3 = 0$, $n_1 + n_2 + n_3 = N$.

Appendix B: Scalling of the CFI entries

In this section, we will show that: For a final state $|\psi\rangle_f$ with $\tau = 2\pi/9$, there exist parameters $\boldsymbol{\theta}_{G_N}$ with $\theta_1 = \theta_2 = (1 + 1/N)2\pi/3$, such that the QFI entries

$$F_{11}^c = F_{22}^c = \frac{2N^2}{3}, F_{12}^c = -\frac{N^2}{3}. \quad (B1)$$

Firstly, we begin with the cases where the total particle number $N = 3k$, $k \in \mathbb{N}$. Set $N\theta_1 = N\theta_2 = 2\pi/3$, we have the probability

$$P_n = \frac{N!}{3^{N+1} n_1! n_2! n_3!} \left\{ 3 + 2 \cos \left[\frac{2\pi}{3} (n_2 - n_3 + 1) \right] + 2 \cos \left[\frac{2\pi}{3} (n_1 - n_3 + 1) \right] + 2 \cos \left[\frac{2\pi}{3} (n_1 - n_2) \right] \right\}, \quad (B2)$$

and the derivatives

$$\partial_1 P_n = \frac{N! N}{3^{N+1} n_1! n_2! n_3!} \left\{ -2 \sin \left[\frac{2\pi}{3} (n_1 - n_3 + 1) \right] - 2 \sin \left[\frac{2\pi}{3} (n_1 - n_2) \right] \right\}, \quad (B3)$$

$$\partial_2 P_n = \frac{N! N}{3^{N+1} n_1! n_2! n_3!} \left\{ -2 \sin \left[\frac{2\pi}{3} (n_2 - n_3 + 1) \right] + 2 \sin \left[\frac{2\pi}{3} (n_1 - n_2) \right] \right\}. \quad (B4)$$

For simplicity, we further reformulate the CFI entries as

$$F_{\mu\nu}^c = N^2 \sum_{n_1, n_2} \frac{N!}{3^{N+1} n_1! n_2! n_3!} f_{\mu\nu}^{(n)}, \quad (B5)$$

with

$$f_{\mu\nu}^{(\mathbf{n})} = \frac{3^{N+1} n_1! n_2! n_3!}{N! N^2} \frac{\partial_\mu P_{\mathbf{n}} \partial_\nu P_{\mathbf{n}}}{P_{\mathbf{n}}}. \quad (\text{B6})$$

The value of $f_{\mu\nu}^{(\mathbf{n})}$ only depend on $(\mathbf{n} \bmod 3)$. We list them as follows:

$\mathbf{n} \bmod 3$	(0,0,0)	(0,1,2)	(0,2,1)	(1,0,2)	(1,1,1)	(1,2,0)	(2,0,1)	(2,1,0)
$f_{11}^{(\mathbf{n})}$	1	4	1	1	1	4	4	1
$f_{12}^{(\mathbf{n})}$	1	-2	-2	-2	1	-2	-2	-2
$f_{22}^{(\mathbf{n})}$	1	1	4	4	1	1	1	4

We mention that the coefficient of $f_{\mu\nu}^{(\mathbf{n})}$ in Eq.(B5) is invariant under the permutation $n_1 \rightarrow n_2 \rightarrow n_3 \rightarrow n_1$. Hence, $f_{\mu\nu}^{(\mathbf{n})}$ can be further divided into three types with $\{n_1, n_2, n_3\} \bmod 3 = \{0, 0, 0\}$, $\{1, 1, 1\}$, and $\{0, 1, 2\}$, respectively. And $F_{\mu\nu}^c$ is invariant under the substitution

$$f_{11}^{(\mathbf{n})}, f_{22}^{(\mathbf{n})} \rightarrow 2 - \frac{1}{3} \sum_{i>j} \cos\left[\frac{2\pi}{3}(n_i - n_j)\right], \quad (\text{B7})$$

$$f_{12}^{(\mathbf{n})} \rightarrow \frac{2}{3} \sum_{i>j} \cos\left[\frac{2\pi}{3}(n_i - n_j)\right] - 1. \quad (\text{B8})$$

Because, for a set of given $\{n_1, n_2, n_3\}$ in an arbitrary type of the three, this substitution keeps the average of $f_{\mu\nu}^{(\mathbf{n})}$ in this set invariant. Furthermore, we have the summation:

$$N^2 \sum_{n_1 n_2} \frac{N!}{3^{N+1} n_1! n_2! n_3!} = \frac{N^2}{3}, \quad (\text{B9})$$

and

$$\begin{aligned} & N^2 \sum_{n_1 n_2} \frac{N!}{3^{N+1} n_1! n_2! n_3!} \frac{1}{3} \sum_{i>j} \cos\left[\frac{2\pi}{3}(n_i - n_j)\right] \\ &= \frac{N^2}{3^{N+1}} \sum_{n_1 n_2} \frac{N!}{n_1! n_2! n_3!} \operatorname{Re} \left[(e^{i2\pi/3})^{n_1} (e^{i4\pi/3})^{n_2} (e^{i0\pi/3})^{n_3} \right] \\ &= \frac{N^2}{3^{N+1}} \operatorname{Re} \left[e^{i2\pi/3} + e^{i4\pi/2} + e^{i0\pi/3} \right]^N \\ &= 0. \end{aligned} \quad (\text{B10})$$

Make the substitution B7 and B8 on Eq. (B5), then insert the summation B9 and B10, we have the CFI entries

$$F_{11}^c = F_{22}^c = \frac{2N^2}{3}, F_{12}^c = F_{21}^c = -\frac{N^2}{3}. \quad (\text{B11})$$

As for the cases with particle number $N = 3k + 1$ and $N = 3k + 2$, one can verify it with the same methods.

We have thus shown that for all N , there exist parameters (θ_1, θ_2) , such that the CFIM take the values in Eq. (B1).

-
- [1] C. W. Helstrom, *Quantum Detection and Estimation Theory* (Academic Press, New York, 1976).
[2] A. S. Holevo, *Probabilistic and Statistical Aspect of Quantum Theory* (North-Holland, Amsterdam, 1982).
[3] L. Pezzè, A. Smerzi, M. K. Oberthaler, R. Schmied, and P. Treutlein, Rev. Mod. Phys. **90**, 035005 (2018), and

- references therein.
[4] C. L. Degen, F. Reinhard, and P. Cappellaro, Rev. Mod. Phys. **89**, 035002 (2017), and references therein.
[5] D. Braun, G. Adesso, F. Benatti, R. Floreanini, U. Marzolino, M. W. Mitchell, and S. Pirandola, Rev. Mod. Phys. **90**, 035006 (2018), and references therein.

- [6] LIGO Scientific Collaboration, *Nat. Phys.* **7**, 962 (2011).
- [7] R. J. Sewell, M. Koschorreck, M. Napolitano, B. Dubost, N. Behbood, and M.W. Mitchell, *Phys. Rev. Lett.* **109**, 253605 (2012);
- [8] C. F. Ockeloen, R. Schmied, M. F. Riedel, and P. Treutlein, *Phys. Rev. Lett.* **111**, 143001 (2013);
- [9] W. Muessel, H. Strobel, D. Linnemann, D. B. Hume, and M. K. Oberthaler, *Phys. Rev. Lett.* **113**, 103004 (2014).
- [10] O. Hosten, N. J. Engelsen, R. Krishnakumar, and M. A. Kasevich, *Nature (London)* **529**, 505 (2016);
- [11] I. Kruse, K. Lange, J. Peise, B. Lücke, L. Pezzè, J. Arlt, W. Ertmer, C. Lisdat, L. Santos, A. Smerzi, and C. Klempert, *Phys. Rev. Lett.* **117**, 143004 (2016).
- [12] R. Stevenson, M.R. Hush, T. Bishop, I. Lesanovsky, and T. Fernholz, *Phys. Rev. Lett.* **115**, 163001 (2015).
- [13] Yanming Che, Fei Yao, Hongbin Liang, Guolong Li, and Xiaoguang Wang, *Phys. Rev. A* **98**, 053609 (2018).
- [14] Fei Yao, Yanming Che, Yuguo Su, Hongbin Liang, Jiancheng Pei, and Xiaoguang Wang, *Phys. Rev. A* **99**, 052128 (2019).
- [15] M. D. Vidrighin, G. Donati, M. G. Genoni, X.-M. Jin, W. S. Kolthammer, M. S. Kim, A. Datta, M. Barbieri, and I. A. Walmsley, *Nat. Commun.* **5**, 3532 (2014).
- [16] P. J. D. Crowley, A. Datta, M. Barbieri, and I. A. Walmsley, *Phys. Rev. A* **89**, 023845 (2014).
- [17] P. Kok, J. Dunningham, and J. F. Ralph, *Phys. Rev. A* **95**, 012326 (2017).
- [18] P. C. Humphreys, M. Barbieri, A. Datta, and I. A. Walmsley, *Phys. Rev. Lett.* **111**, 070403 (2013).
- [19] M. Szczykulska, T. Baumgratz, and A. Datta, *Adv. Phys. X* **1**, 621 (2016), and references therein.
- [20] S. Ragy, M. Jarzyna, and R. Demkowicz-Dobrzański, *Phys. Rev. A* **94**, 052108 (2016); Erratum: 99, 029905(E) (2019).
- [21] T. Baumgratz and A. Datta, *Phys. Rev. Lett.* **116**, 030801 (2016).
- [22] L. Pezzè, M. A. Ciampini, N. Spagnolo, P. C. Humphreys, A. Datta, I. A. Walmsley, M. Barbieri, F. Sciarrino, and A. Smerzi, *Phys. Rev. Lett.* **119**, 130504 (2017).
- [23] M. Zhuang, J. Huang, and C. Lee, *Phys. Rev. A* **98**, 033603 (2018).
- [24] M. Gessner, L. Pezzè, and A. Smerzi, *Phys. Rev. Lett.* **121**, 130503 (2018).
- [25] Haijun Xing and Libin Fu, *Phys. Rev. A* **102**, 062613 (2020).
- [26] J. Liu, H. Yuan, X.-M. Lu, and X. G. Wang, *J. Phys. A: Math. Theor.* **53**, 023001 (2020), and references therein.
- [27] X.-M. Lu, and X. G. Wang, *Phys. Rev. Lett.* **126**, 120503 (2021).
- [28] Michael Albiez, Rudolf Gati, Jonas Fölling, Stefan Hunsmann, Matteo Cristiani and Markus K. Oberthaler, *Phys. Rev. Lett.* **95**, 010402 (2005).
- [29] Beilei Zhu, Vijay Pal Singh, Junichi Okamoto and Ludwig Mathey, *Phys. Rev. Research* **3**, 013111 (2021).
- [30] T. Schumm, S. Hofferberth, L. M. Andersson, S. Wildermuth, S. Groth, I. Bar-Joseph, J. Schmiedmayer and P. Krüger, *Nature Phys.* **1**, 57 (2005).
- [31] S. Hofferberth, I. Lesanovsky, T. Schumm, A. Imam-bekov, V. Gritsev, E. Demler, and J. Schmiedmayer, *Nat. Phys.* **4**, 489(2008).
- [32] M. Gring, M. Kuhnert, T. Langen, T. Kitagawa, B. Rauer, M. Schreitl, I. Mazets, D. Adu Smith, E. Demler, and J. Schmiedmayer, *Science* **337**, 1318 (2012).
- [33] T. Berrada, S. van Frank, R. Bücker, T. Schumm, J. Schaff, and J. Schmiedmayer, *Nat. Commun.* **4**, 2077 (2013).
- [34] T. Berrada, S. van Frank, R. Bücker, T. Schumm, J.-F. Schaff, J. Schmiedmayer, B. Julía-Díaz, and A. Polls, *Phys. Rev. A* **93**, 063620 (2016).
- [35] C. Lee, *Phys. Rev. Lett.* **97**, 150402 (2006).
- [36] Y.-J. Wang, D. Z. Anderson, V. M. Bright, E. A. Cornell, Q. Diot, T. Kishimoto, M. Prentiss, R. A. Saravanan, S. R. Segal, and S. Wu, *Phys. Rev. Lett.* **94**, 090405 (2005).
- [37] Y. Shin, M. Saba, T. A. Pasquini, W. Ketterle, D. E. Pritchard, and A. E. Leanhardt, *Phys. Rev. Lett.* **92**, 050405 (2004).
- [38] G.-B. Jo, J.-H. Choi, C. A. Christensen, T. A. Pasquini, Y.-R. Lee, W. Ketterle, and D. E. Pritchard, *Phys. Rev. Lett.* **98**, 180401 (2007).
- [39] G. D. McDonald, H. Keal, P. A. Altin, J. E. Debs, S. Bennetts, C. C. N. Kuhn, K. S. Hardman, M. T. Johnson, J. D. Close, and N. P. Robins, *Phys. Rev. A* **87**, 013632 (2013).
- [40] H. Müntinga, H. Ahlers, M. Krutzik, A. Wenzlawski, S. Arnold, D. Becker, K. Bongs, H. Dittus, H. Duncker, N. Gaaloul, C. Gherasim, E. Giese, C. Grzeschik, T. W. Hänsch, O. Hellmig, W. Herr, S. Herrmann, E. Kajari, S. Kleinert, C. Lämmerzahl, W. Lewoczko-Adamczyk, J. Malcolm, N. Meyer, R. Nolte, A. Peters, M. Popp, J. Reichel, A. Roura, J. Rudolph, M. Schiemanck, M. Schneider, S. T. Seidel, K. Sengstock, V. Tamma, T. Valenzuela, A. Vogel, R. Walser, T. Wendrich, P. Windpassinger, W. Zeller, T. van Zoest, W. Ertmer, W. P. Schleich, and E. M. Rasel, *Phys. Rev. Lett.* **110**, 093602 (2013).
- [41] Karol Gietka and Jan Chwedeńczuk, *Phys. Rev. A* **90**, 063601 (2014).
- [42] M. Zuppardo, J. P. Santos, G. De Chiara, M. Paternostro, F. L. Semião and G. M. Palma, *Phys. Rev. A* **91**, 033631 (2015).
- [43] Sheng-Chang Li and Li-Bin Fu, *Phys. Rev. A* **102**, 033313 (2020).
- [44] Wenjie Liu, Min Zhuang, Bo Zhu, Jiahao Huang and Chaohong Lee, *Phys. Rev. A* **103**, 023309 (2021).
- [45] K. Nemoto, C. A. Holmes, G. J. Milburn and W. J. Munro, *Phys. Rev. A* **63**, 013604 (2000).
- [46] R. Franzosi and V. Penna, *Phys. Rev. A* **65**, 013601 (2001).
- [47] R. Franzosi and V. Penna, *Phys. Rev. E* **67**, 046227 (2003).
- [48] H. Cao, Q. Wang and L. B. Fu, *Phys. Rev. A* **89**, 013610 (2014).
- [49] H. Cao, Q. Wang and L. B. Fu, *Laser Phys.* **25** 065501 (2015).
- [50] D. Leibfried, M. D. Barrett, T. Schaetz, J. Britton, J. Chiaverini, W. M. Itano, J. D. Jost, C. Langer, and D. J. Wineland, *Science* **304**, 1476 (2004).
- [51] M. W. Mitchell, J. S. Lundeen, and A. M. Steinberg, *Nature (London)* **429**, 161 (2004).
- [52] I. Afek, O. Ambar, and Y. Silberberg, *Science* **328**, 879 (2010).
- [53] C. W. Helstrom, *Phys. Lett.* **25A**, 101 (1967).
- [54] X.-M. Lu, Z. Ma and C. Zhang, *Phys. Rev. A* **101**, 022303 (2020).
- [55] Jie Liu and Li-Bin Fu, *Phys. Lett. A* **370**, 17 (2007).
- [56] J. J. Bollinger, W. M. Itano, D. J. Wineland, and D. J. Heinzen, *Phys. Rev. A* **54**, R4649(R) (1996).
- [57] T. Monz, P. Schindler, J. T. Barreiro, M. Chwalla, D.

- Nigg, W. A. Coish, M. Harlander, W. Hansel, M. Henrich, and R. Blatt, Phys. Rev. Lett. **106**, 130506 (2011).
[58] S. D. Huver, C. F. Wildfeuer, and J. P. Dowling, Phys. Rev. A **78**, 063828 (2008).